Journal of Materials Chemistry A

PAPER

View Article Online
View Journal | View Issue

Cite this: J. Mater. Chem. A, 2015, 3, 16183

Towards superior oxygen evolution through graphene barriers between metal substrates and hydroxide catalysts†

Hao-Fan Wang,‡ Cheng Tang‡ and Qiang Zhang*

The oxygen evolution reaction (OER) plays a key role in various sustainable energy systems, such as solar cells, fuel cells and metal–air batteries. The wise integration of transition metal compounds with macroscale current collectors is a promising strategy to achieve OER catalysts with high utilization efficiency. Herein, graphene with superior electron pathways, high surface area, excellent conductive and mechanical properties, and conjugate planes to anchor other phases with good dispersion was employed as the barrier between 3D Ni foam and NiFe-LDHs for 3D monolith electrodes. The as-obtained electrode exhibited a remarkably low onset overpotential of 240 mV, a small overpotential of 325 mV for 10 mA cm^{-2} and a substantially decreased Tafel slope of 44 mV dec^{-1} in 0.1 M KOH. The graphene barrier herein not only provides a novel hydrophobic substrate to modulate the growth of 3D NiFe-LDHs with good dispersion, but also delivers a strongly coupled interface between the active phase and current collectors. Consequently, the as-obtained graphene mediated 3D monolith electrode exhibited a very high electrochemically active surface area, an optimal interfacial junction, as well as superior OER performance. This work provides a novel catalyst for OER and more importantly, it reveals the role of graphene in modulating the interfacial features of various composites, which is general and can be employed in many material systems for satisfactory applications in heterogeneous catalysis, energy conversion and storage, sensors and so on.

Received 9th May 2015
Accepted 1st July 2015

DOI: 10.1039/c5ta03422a

www.rsc.org/MaterialsA

1. Introduction

Energy systems based on fossil fuels and biomass, which are the lifeblood of modern society originally come from solar energy, captured and transformed through photosynthesis. However, the low photosynthetic efficiency and sluggish transformation process lead to a gradual diminution of fossil fuels, and the resultant CO_2 emissions are regarded as the main factor towards climate change. Consequently, developing an alternative and sustainable energy system is urgent to meet the requirements of today's society. Artificially converting water and carbon dioxide into oxygen and organics is of great promise for mitigating the energy crisis, and enhancing material circulation in the global ecosystem. The oxygen evolution reaction (OER, $4OH^- \rightarrow O_2 + 2H_2O + 4e^-$ in alkaline solution, with an equilibrium potential of 1.23 V *vs.* reversible hydrogen electrode, RHE) is demonstrated to play a key role in this energy cycle, while suffers from sluggish kinetics and high overpotentials.[1]

To make the OER process more efficient for practical applications, various kinds of catalysts have been designed and applied in this reaction. Noble metals and their oxides are commonly acknowledged as the most highly efficient OER electrocatalysts,[2] but their applications are hindered by their high cost and poor durability. Recently, non-precious metals and their compounds (Fe, Co, Ni, Mn, *etc.*),[3–12] the OER activity of which is demonstrated to compete with that of noble metal oxides such as RuO_2 and IrO_2 [13] on computational volcano curves, have attracted great attention as a family of promising alternatives. Among them, layered double hydroxides (LDHs),[3–7] especially NiFe and NiCo LDHs,[3–6,10] are widely investigated and recognized as the most highly active catalysts for OER. In these studies, the catalysts were generally dropped onto the working electrode, and adhered to it by the aid of binders. It's notable that the catalysts will easily flake off due to the oxygen bubbles generating and escaping from the surface constantly during the OER process, thereby resulting in low durability and unstable performance. Aiming at this problem, some recent studies employed Ni foam as a three-dimensional (3D) porous and conductive substrate.[6,11] *Via in situ* nucleation and growth, hierarchical LDH sheets were grown from and anchored onto the Ni substrate to serve as freestanding working electrodes directly.

Beijing Key Laboratory of Green Chemical Reaction Engineering and Technology, Department of Chemical Engineering, Tsinghua University, Beijing 100084, PR China. E-mail: zhang-qiang@mails.tsinghua.edu.cn

† Electronic supplementary information (ESI) available: SEM images, TEM images, EDS pattern, TGA plots, and chronoamperometric response of LDH based catalysts, the morphology evolution of G/Ni during the OER process, and a summary of the OER performances of transition metal compound based catalysts. See DOI: 10.1039/c5ta03422a

‡ H. F. Wang and C. Tang contribute equally.

In spite of a 3D hierarchical structure and binder-free preparation, poorly conductive LDH sheets packed and banked on the Ni substrate surface, which resulted in limited electron transportation through the catalytic phase and insufficient utilization of active sites. Consequently, the fine arrangement of LDH sheets on Ni substrates and the interfacial modulation still remain challenges towards a high efficiency and full demonstration of LDH/Ni systems for OER electrocatalysis.

In this contribution, an ultrathin graphene layer was introduced to modulate the growth behaviors and catalytic performances of NiFe LDHs on the Ni foam substrate (denoted as LDH/G/Ni), as illustrated in Scheme 1. The incorporation of graphene with a high surface area and excellent performance on electron transport is believed to be an effective solution to enhance the electrical conductivity and dispersion of LDHs.[3,12,14] Besides, the graphene layer served as a barrier between the Ni substrate and the precursor solution of LDHs, which appropriately suppressed the subsequent growth of LDH sheets. Moreover, the atom-thick layer of graphene still retained an adequately strong interaction between LDHs and the Ni substrate, and the rich valence states of Ni (Ni^0, Ni^{2+}, Ni^{3+}) are believed to contribute to a low OER onset potential.[15] Consequently, the novel LDH/G/Ni complex was demonstrated to exhibit an excellent OER performance with a low onset overpotential of 240 mV and a greatly decreased Tafel slope of 44 mV dec^{-1}.

2. Results and discussion

Structure of the graphene barrier mediated OER catalyst

To obtain this hybrid material, a continuous layer of graphene was first grown on Ni foam by a chemical vapor deposition (CVD) method in advance[16] and then NiFe LDHs were fabricated on graphene by a hydrothermal coprecipitation method (Scheme 1). Nickel and iron nitrate were fed into the hydrothermal reactor at a mole ratio of 3 : 1. Methanol was utilized as the alkali source instead of common urea to mitigate the corrosion of the Ni foam and surfactant cetyltrimethylammonium bromide (CTAB) was introduced to obtain more uniform LDH sheets.[17] Meanwhile, a complex of NiFe LDHs and Ni foam without graphene (LDH/Ni) was also synthesized under otherwise identical conditions. In the low magnification scanning electron microscopy (SEM) image of G/Ni shown in Fig. 1a, a continuous thin layer of graphene was observed to attach on the Ni foam. After LDH growth, the Ni framework retained its structural integrity without any crush or corrosion, and uniform LDHs were decorated on graphene above the Ni substrate (Fig. 1b). Notably, during LDH growth, interspersed LDH seeds first nucleated all over the surface of graphene in G/Ni, and then gradually grew into small LDH clusters as shown in Fig. 1c, while in the case of LDH/Ni, swarms of LDHs quickly generated on the surface of Ni resulting in continuous covering of the substrate (Fig. S1†). This distinct nucleation and growth behaviour was rationalized by the introduction of hydrophobic, low-defective graphene layers, which increased the LDH nucleation resistance, as well as prevented Ni foam from dissolving and serving as the nickel source for LDHs, thus moderately suppressing the LDH nucleation and the vertical growth of LDH sheets. The impact of graphene hydrophobicity was further supported by the different morphologies of LDHs fabricated on graphene substrates with a hydrophobicity gradient (Fig. S2†). This loose arrangement of LDHs ensured free space for oxygen transport, electrolyte penetration, and easily accessible active sites; meanwhile, the graphene underlayer linked up all the separated LDH sheets with an interconnected electron pathway.

The as-grown LDH sheets were so thin that they were nearly transparent under transmission electron microscopy (TEM, Fig. 1d) with a fringe spacing of 0.25 nm in accordance with the (012) lattice plane of NiFe LDHs (Fig. 1e), and interconnected to form flower-like clusters as shown in SEM (Fig. 1c). Graphene could also be detected by TEM (Fig. 1f), together with LDH sheets. The TEM sample was prepared by an ultrasonic method. Even after a strong ultrasonic treatment for 60 min at a high power (300 W, 40 kHz), the LDH/G/Ni block exhibited no significant change, and only several clusters of LDH and graphene could be observed on the micro-grid. This phenomenon indicated a strong couple interaction between NiFe LDHs and the Ni substrate with a thin graphene layer in-between. The

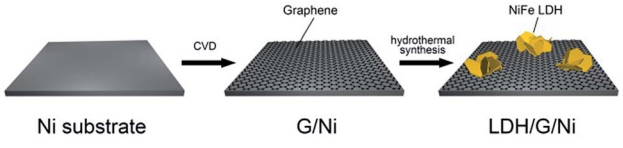

Scheme 1 Synthesis of LDH/G/Ni electrocatalysts with a graphene barrier between Ni substrates and layered NiFe hydroxides.

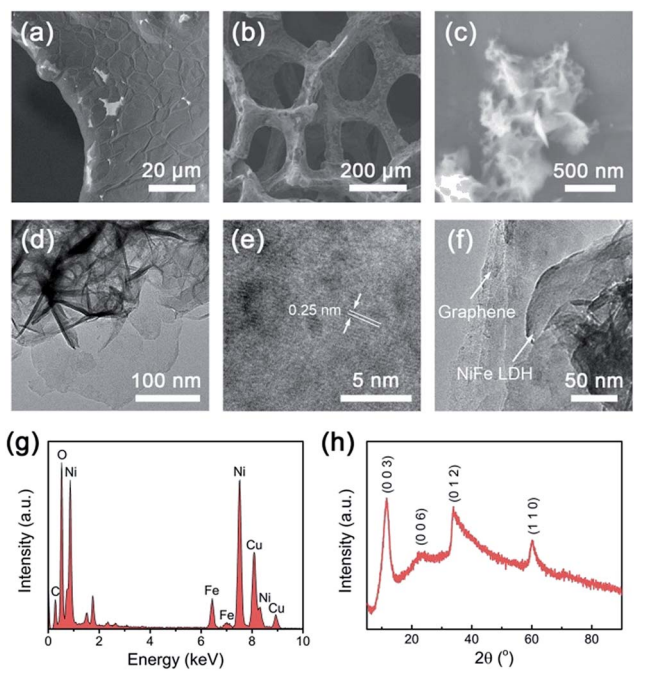

Fig. 1 Characterization of LDH/G/Ni electrocatalysts. (a) SEM image of G/Ni. (b and c) SEM images of LDH/G/Ni, showing interspersed LDH sheets on G/Ni. (d and e) TEM images of NiFe LDHs from LDH/G/Ni electrocatalysts. (f) TEM image of NiFe LDHs and graphene. (g) EDS pattern of NiFe LDHs. (h) XRD pattern of p-LDH.

elemental composition of LDH sheets in Fig. 1d was measured by using an energy dispersive spectrometer (EDS, Fig. 1g) with a mole ratio of Ni/Fe to be 6.0 : 1, much higher than that of the feedstock, which was probably due to the slight dissolution and Ni supply from the Ni foam. For further study of the LDH crystal structure, an X-ray diffraction (XRD) test was performed. However, the as-grown NiFe LDHs were difficult to separate from Ni foam, so the LDH precipitate (p-LDH) in the hydrothermal reactor was utilized as the substitute for the XRD test. The TEM image and EDS pattern revealed that p-LDH exhibited a similar morphology and composition to LDH grown on Ni foam (Fig. S3†). The XRD pattern (Fig. 1h) of p-LDH showed obvious peaks at $2\theta = 11.4°$, 23.0°, 34.4°, and 60.0°, representing the (003), (006), (012), and (110) planes of the NiFe LDH crystal. The above results indicated the successful fabrication of a LDH/G/Ni hybrid with graphene incorporation to regulate the growth behaviors and interfacial interaction of LDHs and the Ni substrate.

OER electrocatalytic performance

To investigate the OER catalytic activity of LDH/G/Ni, it was employed as the working electrode in a three electrode system. Owing to the stable 3D structure of the Ni foam and the conductive scaffold, no binder or additional substrate was required. All electrochemical experiments were performed in 0.1 M KOH solution in comparison with LDH/Ni and G/Ni. The linear sweep voltammetry (LSV) plots at a scan rate of 10 mV s^{-1} are presented in Fig. 2a. The values of the OER current density are directly associated with the reaction process and thereby catalyst activities. With the highest current density, LDH/G/Ni exhibited a superior performance to the contrast samples. The rise of the current at an overpotential of around 0.2 V is assigned to the oxidization current of Ni, and for those samples containing LDH, it also includes the Ni^{2+}/Ni^{3+} redox current. In the LSV test of G/Ni, the silver foam turned black at high overpotential (Fig. S4†), indicating the generation of nickel hydroxides, which was demonstrated to be active for OER catalysis.[18] Additionally, the NiOOH phase generated by the Ni^{2+}/Ni^{3+} transformation is believed to be crucial to the working active sites of LDH during the OER process.[9] Hence, these two oxidation processes, as represented by the redox peak around 0.2 V, were expected to bring about an enhancement in the OER activity, which was supported by the fact that the higher the redox current, the better the OER performance for LDH/G/Ni.

It is noteworthy that in the LSV plot of LDH/G/Ni, the potential ranges for catalyst oxidation and oxygen evolution are partly overlapped, which makes it quite difficult and system-specific to determine the accurate onset potential and Tafel slope as well. To decouple these two reactions, a chronoamperometric testing method was devised to obtain sole OER current densities at specific overpotentials (see ESI† for details). With this method, the onset overpotentials (η_{onset}) of LDH/G/Ni, LDH/Ni, and G/Ni were determined to be 0.24, 0.25, and 0.30 V (Fig. 2b). Fig. 2c exhibits the Tafel plots derived from the data in Fig. 2b. LDH/G/Ni also delivered the smallest Tafel slope (44 mV dec^{-1}), while the Tafel slopes for LDH/Ni and G/Ni were

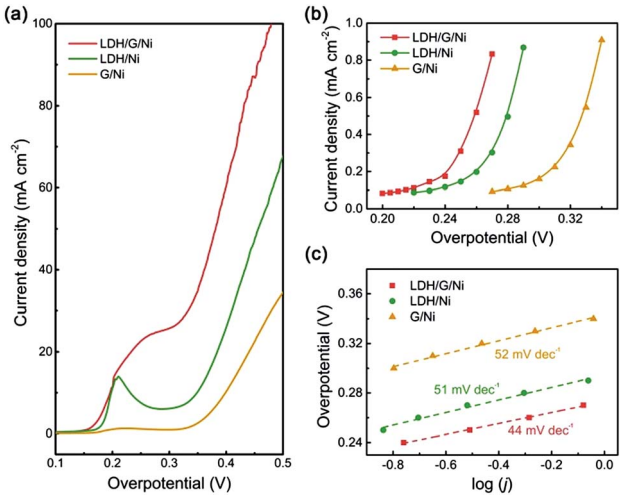

Fig. 2 OER performances of LDH/G/Ni electrocatalysts. (a) *i*–*R* compensated LSV curves. The scan rate was 10 mV s^{-1}. (b) Voltammetric curves obtained by a chronoamperometric method. (c) Tafel plots. All the measurements were performed in O_2 saturated 0.1 M KOH solution.

51 and 52 mV dec^{-1}, respectively. The small Tafel slope of LDH/G/Ni indicated a lower electrochemical polarization. Besides the onset overpotential and Tafel slope, the overpotential required to reach a current density of 10 mA cm^{-2} (η_{10}) and the current density at $\eta = 350$ mV (j_{350}), which are related to the promising OER application of a solar water splitting device,[19] are also two important parameters. As summarized in Table 1, the LDH/G/Ni composite exhibited undoubtedly the best performances compared with other samples, and also among the best results in recent reports (Table S1†).

Relationship between the 3D structure and OER activity

Efficient catalysts for OER require not only sufficient active sites, but also a specific hierarchical structure as well as a strongly coupled interface between supports and active sites. Taking the different structural features into consideration, it is rational to conclude that in addition to the intrinsic catalytic activity of NiFe LDHs and the 3D scaffold of Ni foam, the introduction of graphene tunes the interfacial characters of LDH/Ni with a more active state and enhanced electron transfer, thereby boosting up the OER activity. Detailed discussion is

Table 1 Summary of the OER performances of LDH/G/Ni, LDH/Ni and G/Ni

Samples	η_{onset} (mV)	η_{10}[a] (mV)	j_{350} (mA cm^{-2})	Tafel slope (mV dec^{-1})
LDH/G/Ni	240	325	34.8	44
LDH/Ni	250	350	10.3	51
G/Ni	300	399	2.6	52

[a] The η_{10} for LDH/G/Ni and LDH/Ni can't be obtained from LSV plots. Just like the onset potential, η_{10} was measured by the chronoamperometric method as discussed in the ESI.

conducted to elucidate the relationship between the structure and function for the LDH/G/Ni catalyst.

On one hand, NiFe LDH sheets, as active phases for OER, possess some beneficial structural features to this process. LDH is a kind of anion intercalated hydroxide, thus presenting excellent hydrophilicity. Fig. 3a shows the contact angle tests of LDH/G/Ni and G/Ni tablet samples using deionized water as the wetting liquid. With the introduction of LDHs, the contact angle was greatly decreased from 103.0° to 60.4°, demonstrating a remarkably improved surface wettability and thereby an enhanced electrolyte permeation and affinity. It was further confirmed by the measurement of the electrochemically active surface area (ECSA). Fig. 3b describes the plots of the double-layer capacitance (C_{dl}) test. The slope of each fitting line, equal to twice the C_{dl} of the corresponding material, is proportional to the ECSA.[19] Notably, besides G/Ni, the ECSA of LDH/G/Ni was also higher than that of LDH/Ni, which suggested that the hydrophobic but highly conductive graphene layer improved the interfacial interaction and electrocatalysis during the OER process.

On the other hand, the graphene layer, as an assistance of the 3D porous conductive network constructed by LDHs and the Ni substrate, facilitated the Ni^{2+}/Ni^{3+} redox during the linear sweep process (Fig. 2a). The high resolution Ni 2p spectra of LDH/G/Ni exhibited a *ca.* 0.4 eV shift to higher binding energy compared with LDH/Ni (Fig. 3c), which indicated that the graphene interface modulated the local electronic structure of Ni cations, and thus significantly promoted the OER activity of LDH/Ni. In addition, the graphene layer modulated the growth of LDHs and promoted its dispersion with a higher ECSA. A more uniform and less dense decoration of LDH sheets on the substrate is expected to fully expose the active sites and deliver a much higher utilization efficiency of active sites. Fig. 3d compares the specific current densities based on the loading amount of LDHs for LDH/G/Ni and LDH/Ni. The LDH loading amount was obtained by a thermogravimetric analysis (TGA, Fig. S5†). The greatly higher current density of LDH/G/Ni indicated an improved utilization efficiency of NiFe LDHs with the existence of graphene. In the case of LDH/Ni, the LDH sheets grown on the Ni substrate were so serried and packed that part of the active sites were inaccessible and unutilized, even with a much higher hydrophilicity (Fig. S6†). Thus, graphene not only promoted the OER activity of NiFe LDHs, but also ensured a high utilization efficiency of active sites in LDH/G/Ni. Additionally, distinguished from the reported inorganic/nanocarbon hybrid electrocatalysts,[5,20] the characteristic Ni substrate of LDH/G/Ni serves as a stable scaffold and a macroporous current collector, thus enhancing the OER performance.

Furthermore, the *in situ* growth of NiFe LDHs on graphene above the Ni substrate delivered a strong interfacial connection. To confirm it, a physical mixture of NiFe LDHs and G/Ni with the same LDH loading amount as that of LDH/G/Ni was fabricated, named as LDH + G/Ni, and Nafion was utilized as the binder. It's mentioned above that after a strong ultrasonic treatment for 60 min, the LDH/G/Ni block exhibited no significant change. In contrast, for LDH + G/Ni, the LDH sheets were washed off after the same treatment. As the LSV plots shown in

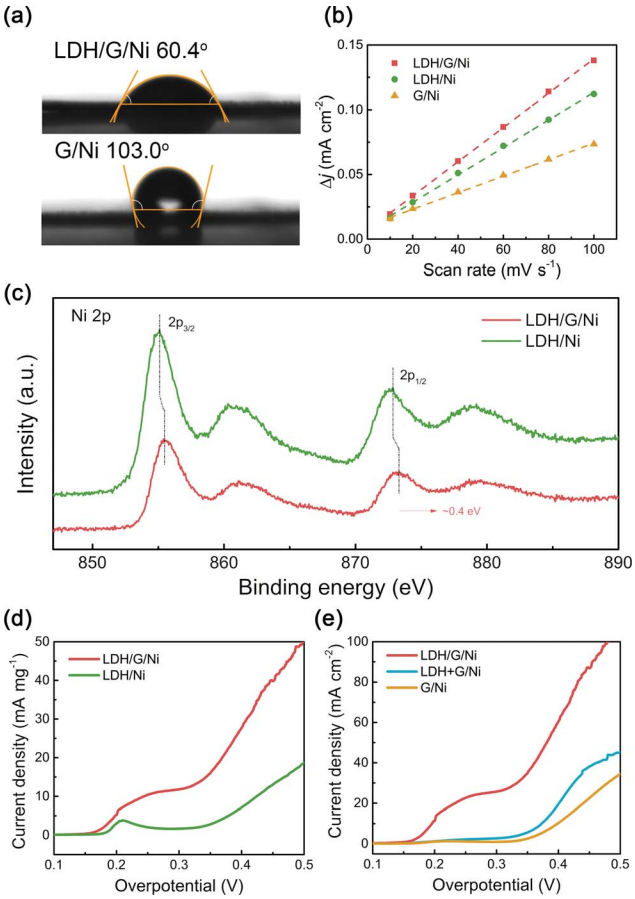

Fig. 3 Characterization of LDH/G/Ni electrocatalysts. (a) Contact angle tests of LDH/G/Ni and G/Ni electrocatalysts. (b) Charging current density differences plotted against scan rates. The linear slope, equivalent to twice the double-layer capacitance C_{dl}, was employed to represent the ECSA. (c) High resolution Ni 2p spectra of LDH/G/Ni and LDH/Ni. (d) LSV plots of LDH/G/Ni and LDH/Ni. The specific current was calculated based on the loading amount of LDHs. (e) LSV plots of LDH/G/Ni, LDH + G/Ni and G/Ni. The scan rate for LSV plots was 10 mV s^{-1}. All the electrocatalytic tests were performed in O_2 saturated 0.1 M KOH solution.

Fig. 3e, LDH/G/Ni dramatically surpassed LDH + G/Ni. Meanwhile, the strong interaction was also demonstrated to enhance the stability of the catalyst (Fig. S7†), and after a long period of OER catalysis, the morphology of LDH/G/Ni mostly remained unchanged (Fig. S8†). During an 8000 s chronoamperometric test, LDH/G/Ni showed high stability comparable to LDH/Ni, indicating that the interfacial connection between LDHs and Ni with an ultra-thin graphene barrier was as strong as the direct connection between LDHs and Ni. The strongly coupled interface between LDH and graphene firmly anchored the LDH sheets and also facilitated the electron transfer from the active phase to graphene and the Ni substrate, thus substantially improving catalysis performances.

The LDH/G/Ni complex was demonstrated to exhibit a superior and greatly enhanced OER catalysis activity, which was contributed from the novel structural features, especially the graphene incorporation. First, the hydrophobic graphene modulated the growth behaviors of LDH on the substrate

towards a uniform decoration, full accessibility and higher utilization efficiency of active sites. Second, the highly conductive graphene layer in-between LDH and the Ni substrate tuned the surficial physical or chemical characters and active states of both components, thereby improving the activity. The use of graphene synthesized from graphene oxide reduction[21] or CVD growth[22,23] is also reported to tune the interaction between the metal support and active electrode (Ni_3S_2/Co_3S_4,[21] nickel cobalt binary hydroxides,[22] or NiO[23]) for supercapacitors. Herein, the ultrathin graphene ensured a strong connection between LDHs and the Ni substrate, which served as a rapid electron pathway for superior OER reactivity.

3. Conclusions

A graphene barrier mediated hydroxide catalyst was proposed and exploited as a greatly effective OER electrode. With a regulated LDH hybridization, fully-exposed active sites, and a strongly coupled interface attributed to the incorporation of graphene, the well-designed 3D hierarchical electrode exhibited superior OER performance with a small onset overpotential of 240 mV, a low overpotential of 325 mV for 10 mA cm^{-2} and a decreased Tafel slope of 44 mV dec^{-1} in 0.1 M KOH. This work is helpful for the exploration of more efficient OER catalysts, and is also expected to inspire more research on the employment of graphene to modulate the interfacial features of various composites towards satisfactory applications in heterogeneous catalysis, energy conversion and storage, sensors and so on.

4. Experimental section

Synthesis of OER catalysts

Ni foam was cut into small pieces of 1 × 1 cm, and cleaned in an ultrasonic washer using ethanol and deionized water for 10 minutes, orderly. The growth of porous graphene was carried out in a tube furnace by a CVD method.[24] Several pieces of cleaned Ni foam were placed in a quartz boat and then placed in the center of a horizontal quartz tube. The tube was then inserted into a furnace at atmospheric pressure. Under the protection of Ar (flow rate: 200 mL min^{-1}), the reactor was heated to 1000 °C, and then H_2 (100 mL min^{-1}) was introduced into the quartz tube for 5 minutes to reduce the oxide layer. After the hydrogen treatment, 20 mL min^{-1} CH_4 was fed into the reactor for 5 minutes. Then the reactor was rapidly cooled to room temperature in the protection of Ar flow. The G/Ni foam was finally collected for further use.

The as-prepared graphene/Ni foam was then put into a 50 mL Teflon autoclave. A solution of 0.45 mmol $Ni(NO_3)_2 \cdot 6H_2O$, 0.15 mmol $Fe(NO_3)_3 \cdot 9H_2O$, 1.0 g CTAB, 6.5 g water and 25.0 g methanol was decanted into the autoclave. This hydrothermal synthesis reactor was heated at 180 °C for 24.0 h to enable the growth of NiFe LDH. At 180 °C, methanol and nitrate ions react as follows: $4CH_3OH + NO_3^- \rightarrow 4HCHO + NH_3 + OH^- + H_2O$.[17] Hydroxyl ions were released slowly, favorable to the uniform growth of NiFe LDH. After the hydrothermal treatment, LDH/G/Ni was ultrasonically cleaned with deionized water for 10 minutes, and then dried at room temperature for the following experiments. The LDH precipitate in the reactor was washed using deionized water in a suction filter, and then preserved after natural drying.

The LDH/Ni catalyst was synthesized using pure Ni foam by the same method. The loading amount of LDHs on LDH/G/Ni and LDH/Ni is 2.18 and 3.63 mg cm^{-2}, respectively.

The LDH + G/Ni catalyst was obtained by dropping LDH suspension onto G/Ni foam. The suspension was prepared by mixing 5.0 mg p-LDH with 0.95 mL ethanol and 0.05 mL Nafion solution, and then 1.0 h ultrasonic treatment was applied to make the suspension more homogeneous. The dropping amount was determined by the LDH quantity on LDH/G/Ni. After the Ni foam was dried, the LDH was adhered on its surface.

Structural characterization

The morphology of the electrocatalysts was characterized using a JSM 7401F scanning electron microscope (SEM) operated at 3.0 kV and a JEM 2010 high-resolution transmission electron microscope (TEM) operated at 120.0 kV. Energy dispersive spectroscopy (EDS) analysis was performed at an acceleration voltage of 120.0 kV using a JEM 2010 TEM equipped with an Oxford Instrument energy dispersive spectrometer. The loading amount of LDH on LDH/G/Ni and LDH/Ni was obtained through a thermogravimetric analysis (TGA) by using a TGA/DSC1 STARe system under N_2 flow. X-ray diffraction (XRD) patterns were recorded on a Bruker D8 Advance diffractometer at 40.0 kV and 120 mA with Cu-K_α radiation. The contact angle was measured on an OCAH200 Optical contact angle measuring instrument (Dataphysics, Germany). The X-ray photoelectron spectroscopy (XPS) measurement was carried out by Escalab 250xi.

Electrochemical performance evaluation

All electrochemical measurements were performed in a three-electrode system, using a Pt sheet as the counter electrode and a saturated calomel electrode (SCE) as the reference electrode. Ni foam fastened to an electrode clip was used as the working electrode. This three-electrode system was controlled by a CHI 760D electrochemical workstation (CH Instrument, USA) and the measurements were carried out in O_2-saturated 0.1 M KOH solution. Before other measurements were performed, the catalyst was cycled several times by cyclic voltammetry (CV). OER activities were tested by linear sweep voltammetry (LSV) at a scan rate of 10 mV s^{-1}. 95% *iR*-compensation was applied during LSV and chronoamperometric tests.

A constant potential was applied on the working electrode to decouple the catalyst oxidation and OER current. The catalyst oxidation current gradually dropped to zero in the first few seconds, and with the increase of time, the current density will eventually approach a constant value, that is, the OER current density at the corresponding potential. By changing the given potential in a suitable region, the correspondence between current density and potential was obtained. For other samples, the same method was employed, and these voltammetry curves

could be substitutes to the LSV plots adjacent to the onset potential.

Electrochemically active surface areas (ECSAs) were determined by measuring the capacitive current associated with double-layer charging from the scan-rate dependence of cyclic voltammetry (CV). This measurement was performed on the same working electrodes in a potential window of 0.85–0.90 V *vs.* RHE and scan rates ranging from 10 to 100 mV s^{-1}. Then linear fitting of the charging current density differences ($\Delta j = j_a - j_c$ at a potential of 875 mV *vs.* RHE) against the scan rate was done. The slope is twice the double-layer capacitance C_{dl}, which is used to represent ECSAs.[19] The durability test was performed at η_{10} (the overpotential for 10 mA cm^{-2}) for each catalyst. The potential *vs.* RHE ($E_{vs.\ RHE}$) was calculated by the following equation: $E_{vs.\ RHE} = E_{vs.\ SCE} + 0.0592\ pH + 0.241$ ($E_{vs.\ SCE}$ stands for the potential *vs.* SCE) and the overpotential $\eta = E_{vs.\ RHE} - 1.229$.

Acknowledgements

This work was supported by the Natural Scientific Foundation of China (no. 21306102 and 21422604) and the Tsinghua University Initiative Scientific Research Program (2014z22076). We thank helpful discussion from Jia-Le Shi and Han-Sen Wang.

Notes and references

1 Y. Jiao, Y. Zheng, M. Jaroniec and S. Z. Qiao, *Chem. Soc. Rev.*, 2015, **44**, 2060.

2 S. Trasatti, *Electrochim. Acta*, 1984, **29**, 1503; A. Rossi and J. F. C. Boodts, *J. Appl. Electrochem.*, 2002, **32**, 735.

3 D. Tang, J. Liu, X. Wu, R. Liu, X. Han, Y. Han, H. Huang, Y. Liu and Z. Kang, *ACS Appl. Mater. Interfaces*, 2014, **6**, 7918; M. Gong, Y. Li, H. Wang, Y. Liang, J. Z. Wu, J. Zhou, J. Wang, T. Regier, F. Wei and H. Dai, *J. Am. Chem. Soc.*, 2013, **135**, 8452.

4 W. Ma, R. Ma, C. Wang, J. Liang, X. Liu, K. Zhou and T. Sasaki, *ACS Nano*, 2015, **9**, 1977; Z. Lu, W. Xu, W. Zhu, Q. Yang, X. Lei, J. Liu, Y. Li, X. Sun and X. Duan, *Chem. Commun.*, 2014, **50**, 6479; B. M. Hunter, J. D. Blakemore, M. Deimund, H. B. Gray, J. R. Winkler and A. M. Muller, *J. Am. Chem. Soc.*, 2014, **136**, 13118; L. Trotochaud, S. L. Young, J. K. Ranney and S. W. Boettcher, *J. Am. Chem. Soc.*, 2014, **136**, 6744; X. Lu and C. Zhao, *Nat. Commun.*, 2015, **6**, 6616; F. Song and X. Hu, *Nat. Commun.*, 2014, **5**, 4477; J. Nai, H. Yin, T. You, L. Zheng, J. Zhang, P. Wang, Z. Jin, Y. Tian, J. Liu, Z. Tang and L. Guo, *Adv. Energy Mater.*, 2015, **5**, 1401880.

5 X. Long, J. Li, S. Xiao, K. Yan, Z. Wang, H. Chen and S. Yang, *Angew. Chem., Int. Ed.*, 2014, **53**, 7584.

6 J. Jiang, A. Zhang, L. Li and L. Ai, *J. Power Sources*, 2015, **278**, 445.

7 X. Long, S. Xiao, Z. Wang, X. Zheng and S. Yang, *Chem. Commun.*, 2015, **51**, 1120; Y. Li, L. Zhang, X. Xiang, D. Yan and F. Li, *J. Mater. Chem. A*, 2014, **2**, 13250; F. Song and X. Hu, *J. Am. Chem. Soc.*, 2014, **136**, 16481; X. Zou, A. Goswami and T. Asefa, *J. Am. Chem. Soc.*, 2013, **135**, 17242.

8 Y. Li, K. Guo, J. Li, X. Dong, T. Yuan, X. Li and H. Yang, *ACS Appl. Mater. Interfaces*, 2014, **6**, 20949; J. Landon, E. Demeter, N. İnoğlu, C. Keturakis, I. E. Wachs, R. Vasić, A. I. Frenkel and J. R. Kitchin, *ACS Catal.*, 2012, **2**, 1793; Y.-F. Li and A. Selloni, *ACS Catal.*, 2014, **4**, 1148; L. Kuai, J. Geng, C. Chen, E. Kan, Y. Liu, Q. Wang and B. Geng, *Angew. Chem., Int. Ed.*, 2014, **53**, 7547; T. Naresh Kumar, S. Sivabalan, N. Chandrasekaran and K. L. Phani, *Chem. Commun.*, 2015, **51**, 1922; A. M. Smith, L. Trotochaud, M. S. Burke and S. W. Boettcher, *Chem. Commun.*, 2015, **51**, 5261; J. Y. C. Chen, J. T. Miller, J. B. Gerken and S. S. Stahl, *Energy Environ. Sci.*, 2014, **7**, 1382; M. W. Louie and A. T. Bell, *J. Am. Chem. Soc.*, 2013, **135**, 12329; L. Wang, C. Lin, D. Huang, F. Zhang, M. Wang and J. Jin, *ACS Appl. Mater. Interfaces*, 2014, **6**, 10172; X. Zhong, H. Yu, G. Zhuang, Q. Li, X. Wang, Y. Zhu, L. Liu, X. Li, M. Dong and J.-g. Wang, *J. Mater. Chem. A*, 2014, **2**, 897; S. Chen and S.-Z. Qiao, *ACS Nano*, 2013, **7**, 10190; J. Wang, T. Qiu, X. Chen, Y. Lu and W. Yang, *J. Power Sources*, 2014, **268**, 341; Y. Hou, Z. Wen, S. Cui, S. Ci, S. Mao and J. Chen, *Adv. Funct. Mater.*, 2015, **25**, 872; S. Chen, J. Duan, M. Jaroniec and S. Z. Qiao, *Angew. Chem., Int. Ed.*, 2013, **52**, 13567; J. Wang, H. X. Zhong, Y. L. Qin and X. B. Zhang, *Angew. Chem., Int. Ed.*, 2013, **52**, 5248; Y. Zhu, W. Zhou, Z. G. Chen, Y. Chen, C. Su, M. O. Tade and Z. Shao, *Angew. Chem., Int. Ed.*, 2015, **54**, 3897; S. Chen, J. Duan, W. Han and S. Z. Qiao, *Chem. Commun.*, 2014, **50**, 207; J. R. Galán-Mascarós, *ChemElectroChem*, 2015, **2**, 37; S. Chen, J. Duan, J. Ran, M. Jaroniec and S. Z. Qiao, *Energy Environ. Sci.*, 2013, **6**, 3693; S. Mao, Z. Wen, T. Huang, Y. Hou and J. Chen, *Energy Environ. Sci.*, 2014, **7**, 609; M. S. Burke, M. G. Kast, L. Trotochaud, A. M. Smith and S. W. Boettcher, *J. Am. Chem. Soc.*, 2015, **137**, 3638; W. Yuan, P. K. Shen and S. P. Jiang, *J. Mater. Chem. A*, 2014, **2**, 123; C. Jin, F. Lu, X. Cao, Z. Yang and R. Yang, *J. Mater. Chem. A*, 2013, **1**, 12170; X. Zhou, Z. Xia, Z. Zhang, Y. Ma and Y. Qu, *J. Mater. Chem. A*, 2014, **2**, 11799; T. Y. Ma, S. Dai, M. Jaroniec and S. Z. Qiao, *J. Am. Chem. Soc.*, 2014, **136**, 13925; M. Zhang, M. de Respinis and H. Frei, *Nat. Chem.*, 2014, **6**, 362; Z. Lu, H. Wang, D. Kong, K. Yan, P. C. Hsu, G. Zheng, H. Yao, Z. Liang, X. Sun and Y. Cui, *Nat. Commun.*, 2014, **5**, 4345; G.-L. Tian, Q. Zhang, B. Zhang, Y.-G. Jin, J.-Q. Huang, D. S. Su and F. Wei, *Adv. Funct. Mater.*, 2014, **24**, 5956; G.-L. Tian, M.-Q. Zhao, D. Yu, X.-Y. Kong, J.-Q. Huang, Q. Zhang and F. Wei, *Small*, 2014, **10**, 2251.

9 D. Friebel, M. W. Louie, M. Bajdich, K. E. Sanwald, Y. Cai, A. M. Wise, M. J. Cheng, D. Sokaras, T. C. Weng, R. Alonso-Mori, R. C. Davis, J. R. Bargar, J. K. Norskov, A. Nilsson and A. T. Bell, *J. Am. Chem. Soc.*, 2015, **137**, 1305.

10 M. Gong and H. Dai, *Nano Res.*, 2014, **8**, 23.

11 Z. Zhao, H. Wu, H. He, X. Xu and Y. Jin, *Adv. Funct. Mater.*, 2014, **24**, 4698.

12 Y. Zhao, S. Chen, B. Sun, D. Su, X. Huang, H. Liu, Y. Yan, K. Sun and G. Wang, *Sci. Rep.*, 2015, **5**, 7629.

13 I. C. Man, H.-Y. Su, F. Calle-Vallejo, H. A. Hansen, J. I. Martínez, N. G. Inoglu, J. Kitchin, T. F. Jaramillo, J. K. Nørskov and J. Rossmeisl, *ChemCatChem*, 2011, **3**, 1159.
14 Z. Wen, S. Ci, Y. Hou and J. Chen, *Angew. Chem., Int. Ed.*, 2014, **53**, 6496; W. Bian, Z. Yang, P. Strasser and R. Yang, *J. Power Sources*, 2014, **250**, 196.
15 W. Zhou, X.-J. Wu, X. Cao, X. Huang, C. Tan, J. Tian, H. Liu, J. Wang and H. Zhang, *Energy Environ. Sci.*, 2013, **6**, 2921.
16 Z. Chen, W. Ren, L. Gao, B. Liu, S. Pei and H. M. Cheng, *Nat. Mater.*, 2011, **10**, 424.
17 H. Chen, L. Hu, M. Chen, Y. Yan and L. Wu, *Adv. Funct. Mater.*, 2014, **24**, 934.
18 M. Gao, W. Sheng, Z. Zhuang, Q. Fang, S. Gu, J. Jiang and Y. Yan, *J. Am. Chem. Soc.*, 2014, **136**, 7077.
19 C. C. McCrory, S. Jung, J. C. Peters and T. F. Jaramillo, *J. Am. Chem. Soc.*, 2013, **135**, 16977.
20 Y. Liang, Y. Li, H. Wang and H. Dai, *J. Am. Chem. Soc.*, 2013, **135**, 2013.
21 D. Ghosh and C. K. Das, *ACS Appl. Mater. Interfaces*, 2015, **7**, 1122.
22 Y. Bai, W. Wang, R. Wang, J. Sun and L. Gao, *J. Mater. Chem. A*, 2015, **3**, 12530–12538.
23 A. Bello, K. Makgopa, M. Fabiane, D. Dodoo-Ahrin, K. I. Ozoemena and N. Manyala, *J. Mater. Sci.*, 2013, **48**, 6707.
24 Z. Chen, W. Ren, L. Gao, B. Liu, S. Pei and H. M. Cheng, *Nat. Mater.*, 2011, **10**, 424.